Current-Mirror-Based Potentiostats for Three-Electrode Amperometric Electrochemical Sensors

Mohammad Mahdi Ahmadi, *Member, IEEE*, and Graham A. Jullien, *Life Fellow, IEEE*

***Abstract*—We present a new circuit topology for potentiostats that interface with three-electrode amperometric electrochemical sensors. In this new topology, a current-copying circuit, e.g., a current mirror, is placed in the sensor current path to generate a mirrored image of the sensor current. The mirrored image is then measured and processed instead of the sensor current itself. The new potentiostat topology consumes very low power, occupies a very small die area, and has potentially very low noise. These characteristics make the new topology very suitable for portable or bioimplantable applications. In order to demonstrate the feasibility of the new topology, we present the results of a potentiostat circuit implemented in a 0.18-μm CMOS process. The circuit converts the sensor current to a frequency-modulated pulse waveform, for which the time difference between two consecutive pulses is inversely proportional to the sensor current. The potentiostat measures the sensor current from 1 nA to 1 μA with better than 0.1% of accuracy. It consumes only 70 μW of power from a 1.8-V supply voltage and occupies an area of 0.02 mm^2.**

***Index Terms*—Amperometric sensor, current mirror, electrochemical sensor, frequency compensation, potentiostat.**

I. Introduction

A THREE-ELECTRODE amperometric electrochemical sensor, shown in Fig. 1, consists of a working electrode (WE), on which an electrochemical reaction takes place; a reference electrode (RE), which is used to measure the solution potential; and a counter electrode (CE), which is an inert conductor supplying the current required for electrochemical reaction at WE [1].

As illustrated in Fig. 1, potentiostat is an electronic instrument that controls the potential difference between WEs and REs at a desired cell potential V_{cell} by injecting the proper amount of current into CE [1].

In this paper, we present a new circuit topology to realize a potentiostat. The new topology is based on the use of a current-copying circuit (e.g., a current mirror), in the path of the sensor current, to generate a mirrored image of the sensor current and then to process the mirrored current instead of the sensor current. To better illustrate the advantages of the new topology over existing topologies, in Section II, we review the basic structure of the prior published potentiostat topologies and briefly explain their advantages and limitations. In Section III, we present the new topology with a few examples of its circuit realization. In Section IV, we discuss the operation of our implemented potentiostat circuit along with a detailed analysis of its frequency compensation. In Section V, we provide the measurement results of our potentiostat circuit and conclude this paper in Section VI.

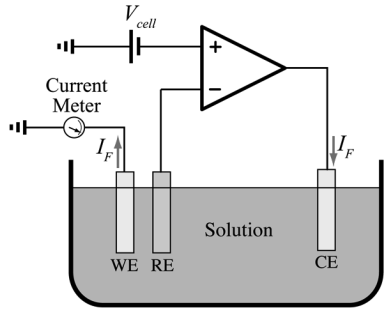

Fig. 1. Conceptual drawing of a three-electrode amperometric electrochemical sensor and a potentiostat.

II. Review of the Existing Potentiostat Topologies[1]

Basically, a potentiostat has two main functions: 1) controlling the potential difference between WE and RE and 2) measuring the current flowing between WE and CE. Each of these functions can be realized with a few different circuit configurations, as summarized in the following subsections.

A. Potential-Control Configurations

The cell potential can be controlled in three configurations [3]: grounded WE; grounded RE; and grounded CE. The first two configurations are electrically the same; thus, in fact, there are really only two different configurations [3].

The grounded-WE configuration is the most popular configuration. Fig. 2 shows the basic implementation of this configuration. As shown, WE is kept at the ground potential, and an operational amplifier, called the control amplifier, controls the

Manuscript received February 25, 2008; revised June 30, 2008. First published September 19, 2008; current version published July 01, 2009. This work was supported in part by the Alberta Informatics Circle of Research Excellence, by Micronet R&D, and by the Natural Sciences and Engineering Research Council of Canada. This paper was recommended by Associate Editor A. van Schaik.

M. M. Ahmadi is with Sound Design Technologies Ltd., Burlington, ON L7L 5P5, Canada (e-mail: mmahmadi@ieee.org).

G. Jullien is with the Department of Electrical and Computer Engineering, University of Calgary, Calgary, AB T2N 1N4, Canada.

Color versions of one or more of the figures in this paper are available online at http://ieeexplore.ieee.org.

Digital Object Identifier 10.1109/TCSI.2008.2005927

[1]Part of the introductory material presented in this section is taken from [2, Ch. 13]. It is included for completeness.

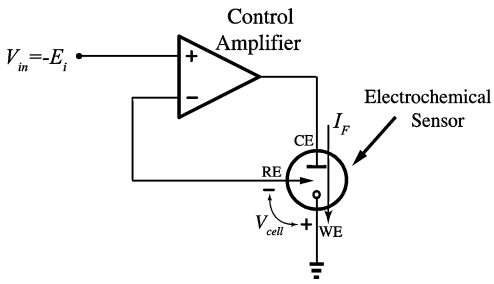

Fig. 2. Potential control using the grounded-WE configuration.

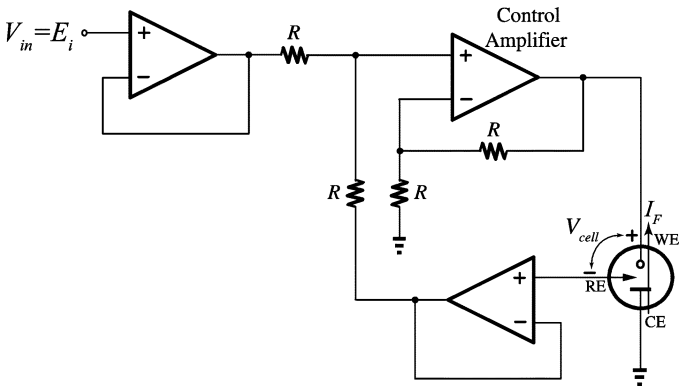

Fig. 3. Potential control using the grounded-CE configuration.

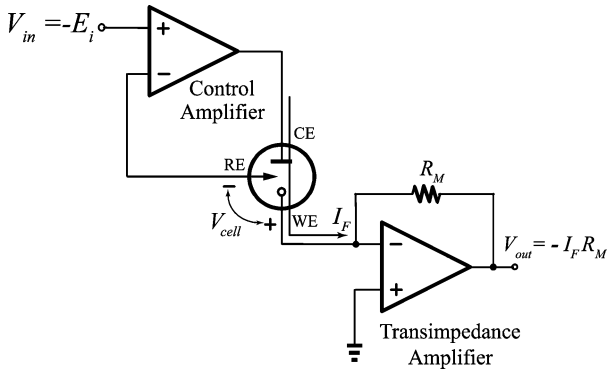

Fig. 4. Current measurement using a transimpedance amplifier.

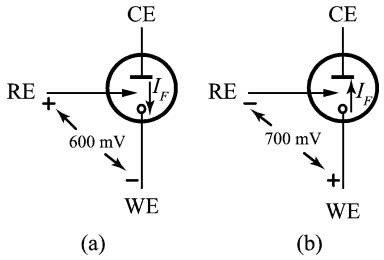

Fig. 5. Cell potential and current direction in (a) O_2-based and (b) H_2O_2-based glucose sensors.

cell current I_F such that the cell potential V_{cell} is kept at its desired preset potential E_i.

The grounded-CE configuration has recently been explored [3] as an alternative for potential control. The basic realization of this configuration is shown in Fig. 3. Clearly, this configuration is more complex and requires more components; thus, it is more vulnerable to component mismatches. However, in cases in which shielding and screening of the WE connection from external electromagnetic interference (EMI) are difficult to implement, using a grounded-CE configuration may improve the current measurement [3].

B. Current Measurement Configurations

A few different configurations exist for measuring the cell current I_F. Here, the current measurement approaches are explained for potentiostats that use a grounded-WE configuration for potential control; however, many of these approaches can be adopted for potentiostats using the grounded-CE configuration.

The use of a transimpedance amplifier is probably the most popular approach for current measurement. In this approach, as shown in Fig. 4, a transimpedance amplifier forces a virtual ground at WE, and at the same time, it generates an output voltage that is linearly proportional to I_F.

This approach has a few advantages [4], [5]. First, it is relatively simple to realize. Second, very small currents can be measured by switching the current measurement resistor R_M to higher values. Third, both potential and current are measured with reference to ground.

The circuit has three major drawbacks [3]–[5]. First, because WE is not connected to a true ground, if its connection to the potentiostat is not carefully shielded, it can pick up environmental noise and interference, particularly high-frequency EMI. This induced noise passes through R_M and produces significant noise levels at the output of the transimpedance amplifier. Second, the input resistance of the transimpedance amplifier behaves inductively [3]–[5]. In other words, at low frequencies, it exhibits a very small impedance; however, as frequency increases, the input impedance increases due to the roll-off in the open-loop gain of the transimpedance amplifier. Since the input impedance is in series with the electrochemical cell, which itself has very large capacitive components, the inductive behavior of the input impedance increases the possibility of instability and oscillation in the potential-control loop.

The third drawback of the circuit appears while working with single supply voltages. This problem can be better explained with reference to two examples.

The two most widely used electrochemical glucose biosensors are oxygen-electrode-based (O_2-based) and hydrogen-peroxide-electrode-based (H_2O_2-based) sensors [6]. In O_2-based glucose sensors, the cell potential V_{cell} should be typically about -600 mV (with reference to a standard Ag/AgCl RE), and the output current of the sensor is the result of the reduction of oxygen at the surface of WE [6]. In other words, as shown in Fig. 5(a), RE (in this case, a Ag/AgCl electrode) is required to be maintained at a potential of about 600 mV above the potential of WE, where the direction of the sensor current is from CE to WE. This means that the output of the transimpedance amplifier must move below the ground potential, which is not possible in single-supply-voltage circuits.

For the H_2O_2-based glucose sensor, the situation is reversed, but the circuit still suffers from the single-supply-voltage issue. In this case, the sensor current is the result of the oxidation of hydrogen peroxide at the surface of WE, and so, as shown in Fig. 5(b), the current flows from WE to CE [6]. However, in this

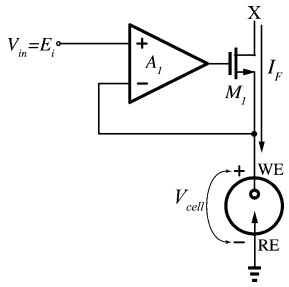

Fig. 6. Potentiostat, designed using a current conveyor, for a two-electrode electrochemical sensor.

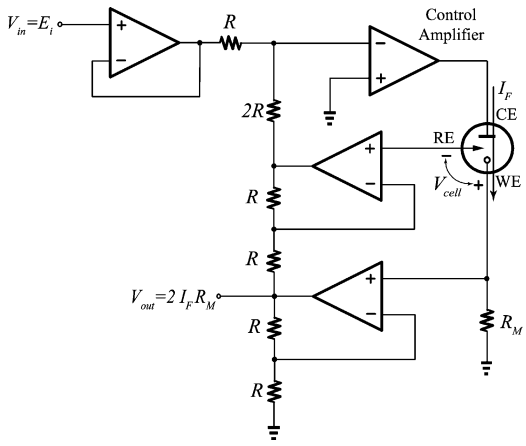

Fig. 7. Current measurement using an inserted resistor in the current path at WE.

case, the cell potential V_{cell} must be typically about 700 mV (assuming a Ag/AgCl RE), meaning that the potential of RE must be kept about 700 mV below the potential of WE, which is again not possible with a single positive supply because WE is held at the lowest potential in the circuit, which is the ground potential.

As a result, with single-supply-voltage circuits, the potential of the noninverting input of the transimpedance amplifier should be raised to an appropriate voltage, depending on the application. This again presents another issue that the measured voltage at the output of the transimpedance amplifier is no longer referenced to ground [2].

Since very large resistors are difficult to realize in integrated-circuit form, the transimpedance amplifier is usually realized with switched-capacitor circuits [7]. In more complicated realizations, the sensor current can be injected directly to a current-input analog-to-digital converter [8] or to a current-input delta–sigma modulator [9], [10].

Using a current conveyor is a similar approach for current measurement, which is widely used for two-electrode sensors [11]–[14]. As shown in Fig. 6, in this approach, WE is held at a virtual ground potential (a low-impedance node), and, instead of converting I_F directly to voltage, it is conveyed from WE to a high-impedance node (X) and is then measured with any of the approaches explained earlier. It is also possible to convert the sensor current to variables other than voltage, such as time [11] or frequency [15].

Another approach for current measurement is to insert a resistor in the current path in WE and measure the voltage developed across that resistor [4]. The voltage can also be amplified before the measurement. Two realizations of this approach are shown in Fig. 7. Clearly, WE is no longer at the ground potential, but its potential changes, depending on I_F. Thus, for proper potential control, the potential is measured and fed back to the control amplifier.

This approach is more complex than using a transimpedance amplifier and requires more active and passive components. As a result, it is noisier and more vulnerable to mismatch between the components. It also has noise and interference pickup issues at WE. However, it is similarly capable of measuring very small currents. Also, both current and voltage are measured with reference to ground.

Yet, another approach for current measurement is to insert a resistor in the current path in CE and measure the voltage generated across that resistor [5]. Fig. 8 shows this approach. As shown, an instrumentation amplifier measures the voltage generated across R_M. Similar to the previous approach, this approach suffers from mismatch in the components; however, it does have a few interesting advantages.

First, because WE is connected to a true ground potential, it is very insensitive to noise and interference pickup. Second, since, excluding the control amplifier, there is no additional active component in the control feedback loop, this circuit has better stability than the previous circuits. Third, both measured voltage and current are referenced to ground.

The last two approaches do not have the problem that the first approach has when working with a single positive voltage. However, these approaches suffer from another issue: As the sensor current increases, the voltage drop across R_M increases, which decreases the headroom for the voltage swing at CE.

III. New Potentiostat Topology

The idea behind the new topology is to interpose a circuit in the path of the sensor current in order to generate a copy of the sensor current and then measure the copied current instead of the sensor current directly.

Fig. 9 shows an implementation of this approach. The operation of the circuit can be explained as follows. The operational amplifier A_1 and transistor M_1 generate a feedback loop through which the potential of RE is stabilized at the desired V_{cell}. Since the circuit is intended to be used in integrated circuits, it is possible to very closely match M_1 and M_2. Since both transistors have the same gate-to-source voltage, the current of M_1 is copied in M_2. An issue, however, is the current mismatch in M_1 and M_2 due to channel-length modulation in those transistors. However, we can minimize this effect by increasing the channel length of those transistors and/or using advanced current-mirror topologies such as cascode or regulated cascade (gain-boosted) circuits.

This potentiostat circuit has important advantages. First, WE is connected to a true ground potential, making it insensitive to noise and interference pickup.

Second, the circuit potentially generates very low noise because it uses fewer active and passive components for measuring

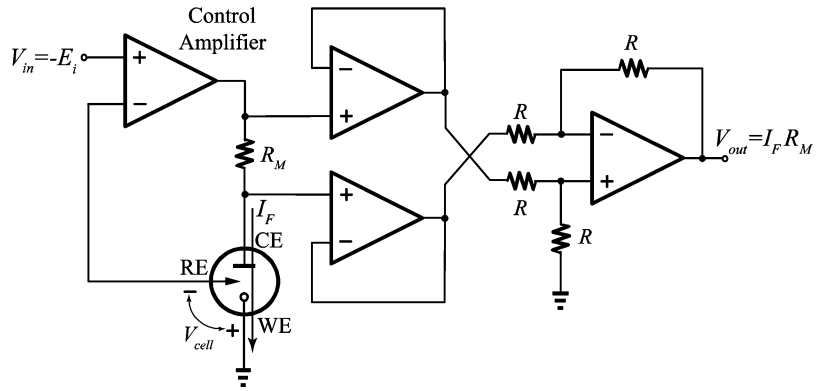

Fig. 8. Current measurement using an inserted resistor in the current path at CE.

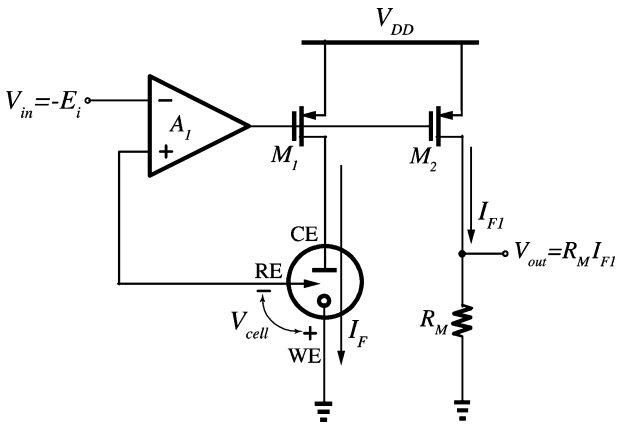

Fig. 9. Current-mirror-based potentiostat.

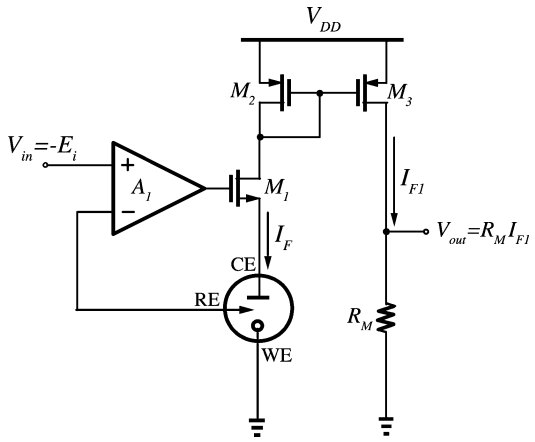

Fig. 10. Improved current-mirror-based potentiostat.

current. In order words, in Fig. 9, only two transistors and one resistor are used for current measurement, whereas in the circuits shown in Section II, at least one resistor and one operational amplifier are used with attendant increases in circuit noise.

Third, the power consumption of the circuit is much lower than that of the circuits described in Section II. Indeed, the added current consumption of the potentiostat for current measurement is equal to the mirrored sensor current, which is negligible.

Fourth, very small currents can be measured by simply switching the current measurement resistor R_M to higher values, and interestingly, this does not have any effect on the stability of the potential-control loop.

In addition to the aforementioned advantages, this circuit does not have the problem with a single supply voltage that affects the operation of the circuit of Fig. 4. Also, the new circuit does not have the voltage headroom issue when measuring large sensor currents, unlike the circuits of Figs. 7 and 8.

Similar to other potentiostat circuits, this circuit might have stability issues when handling very capacitive sensors. As explained previously, this circuit is advantageous in terms of stability because WE is directly connected to ground; however, a disadvantage of this circuit is that another gain stage is added to the potential-control loop. In fact, in this configuration, A_1 and M_1 together constitute the control amplifier of the potentiostat. Assuming that A_1 is a single-stage amplifier, the control amplifier is a two-stage amplifier in which M_1 produces the second stage. Not only the load of this stage vary considerably but also its bias current. If, for example, the goal is to measure the sensor current from 1 nA to 1 μA, then the bias current of M_1 varies in the same range, i.e., three orders of magnitude. As a result, much care should be taken in designing this circuit.

In order to resolve the aforementioned issue, instead of using M_1 as a common-source stage, we can use it in a common-drain (voltage follower) stage, as shown in Fig. 10. This configuration provides much better stability; however, the headroom for the signal swing at CE is reduced because of the $V_{\rm GS}$ drop of M_1. However, this problem can be circumvented using native (zero-threshold voltage) transistors, which are available in almost all of the modern CMOS technologies.

The circuits shown in Figs. 9 and 10 are for sensors in which the output current is the result of a reduction reaction at WE (such as in an O_2-based glucose sensor). In other words, the direction of the sensor current is out of WE. For sensors with oxidation current (such as in a H_2O_2-based glucose sensor), the circuits shown in Fig. 11 should be used. In the circuit shown in Fig. 11(a), the output voltage is referenced to $V_{\rm DD}$. In many applications, this is acceptable. In order to have the output voltage referenced to ground, the circuit shown in Fig. 11(b) can be used.

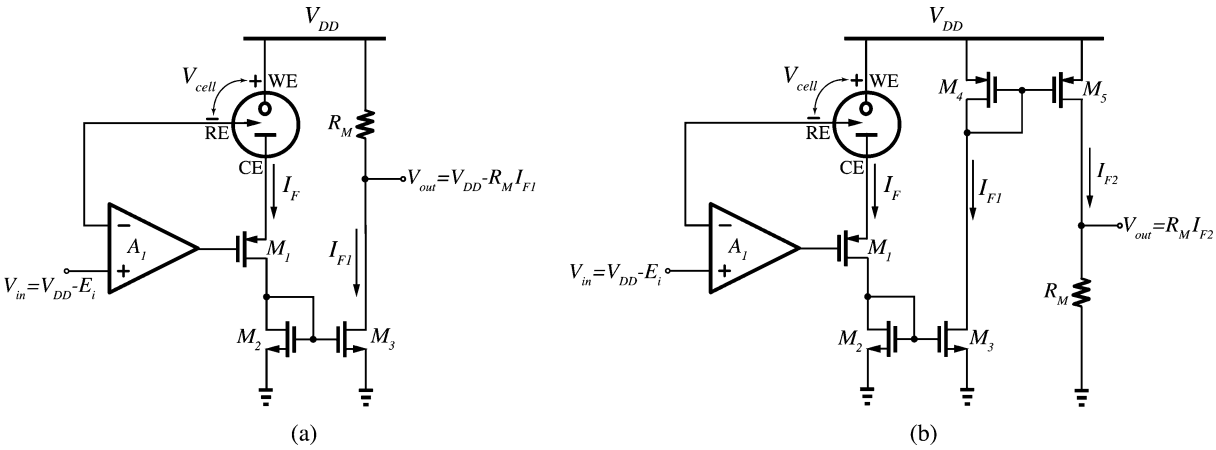

Fig. 11. Current-mirror-based potentiostat for electrochemical sensors with oxidation current. (a) Measuring output voltage with reference to $V_{\rm DD}$. (b) Measuring output voltage with reference to ground.

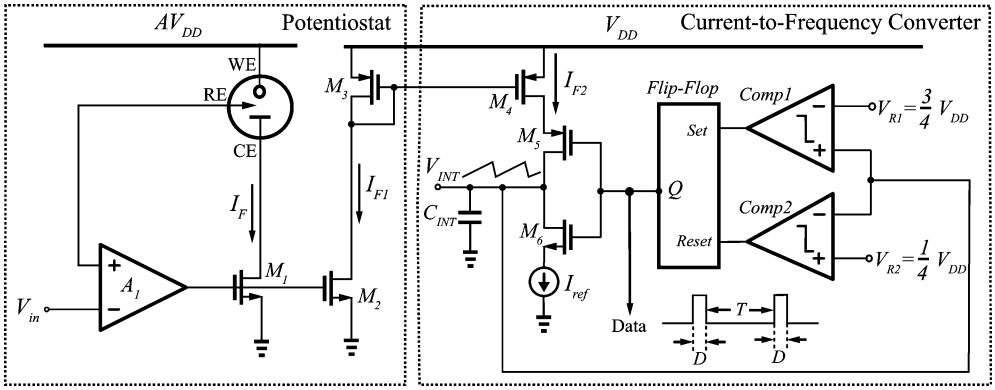

Fig. 12. Simplified schematic of the implemented potentiostat and I-to- F converter.

IV. Circuit Implementation

An integrated potentiostat, based on the approach presented in Section III, was implemented for a transponder chip designed for an implantable microsystem for continuous blood glucose monitoring. The chip was fabricated using the TSMC 0.18-μm CMOS process. Because of system-level considerations, our potentiostat converts the mirrored current to a frequency-modulated pulse waveform, for which the time difference between two consecutive pulses is inversely proportional to the sensor current.

Our potentiostat interfaces with a new electrochemical glucose biosensor developed at the Research Group of Dr. V. Birss in the Department of Chemistry, University of Calgary, Calgary, AB, Canada. The sensor generates an oxidation current at a cell potential of 0.6 V with reference to the standard Ag/AgCl RE.

Fig. 12 shows a simplified schematic of the potentiostat. A_1 and M_1 constitute the potential-control loop. The sensor current is mirrored at M_2 and is injected into a current-to-frequency (I-to-F) converter. To minimize the kickback effect from the I-to-F converter to the potentiostat, the current of M_2 is mirrored again using M_3 and M_4 before it is delivered to the I-to-F converter. A cascode topology is used to realize M_1, M_2, M_3, and M_4 to improve the precision of the current mirrors.

The operation of the I-to- F converter [15] can be seen by assuming that the output of the flip-flop is off, meaning that M_5 is on and M_6 is off. Therefore, the mirrored current of the sensor, namely, I_{F2}, is integrated in $C_{\rm INT}$ until the voltage across $C_{\rm INT}$, namely, $V_{\rm INT}$, exceeds V_{R1}. Then, *Comp1* sets the flip-flop, whereby the reference current $I_{\rm ref}$ starts to discharge $C_{\rm INT}$ until $V_{\rm INT}$ reaches V_{R2}. Finally, *Comp2* resets the flip-flop, and this cycle repeats. Thus, $V_{\rm INT}$ is a sawtooth waveform, and the output of the flip-flop is a low-duty-cycle pulse waveform, for which the time difference between two consecutive pulses, namely, T, and pulsewidth D can be expressed, respectively, by

$$T = \frac{V_{\rm DD} C_{\rm INT}}{2 I_F} \tag{1}$$

$$D = \frac{V_{\rm DD} C_{\rm INT}}{2 I_{\rm ref}}. \tag{2}$$

Thus, T is inversely proportional to I_F, and D is constant.

A. Frequency Compensation of the Potentiostat

Frequency compensation of the potential-control loop of a potentiostat is critical. The load and feedback networks of the control amplifier are generated by the electrochemical cell that often exhibits a highly nonlinear internal impedance. Also, the impedance of electrochemical cells is usually dependent on many variables such as voltage, temperature, concentration of electroactive species, and roughness of electrode surfaces. Therefore, potentiostats should have good stability in order to

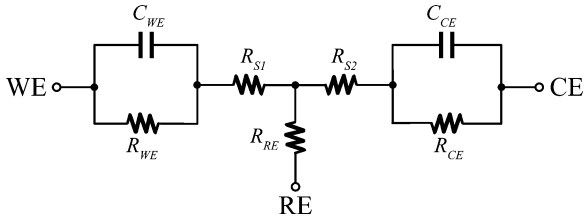

Fig. 13. Generic equivalent circuit of an electrochemical cell.

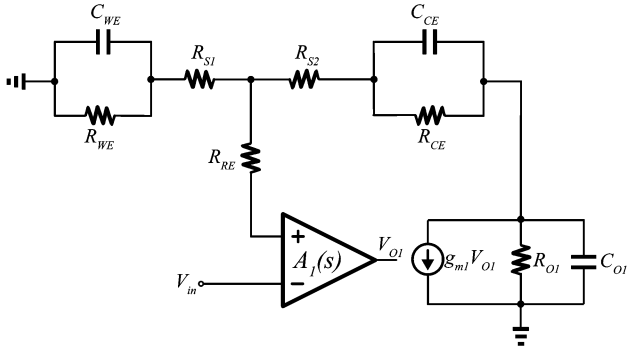

Fig. 14. Small-signal model of the potential-control feedback loop.

successfully handle large load variations during the operation of the sensor.

Fig. 13 shows a generic small-signal equivalent circuit of an electrochemical cell. $C_{\rm CE}$ and $C_{\rm WE}$ represent the double-layer capacitances of the CE and WE, respectively. $R_{\rm CE}$, $R_{\rm RE}$, and $R_{\rm WE}$ represent the charge-transfer resistances of the CE, RE, and WE, and R_{S1} and R_{S2} denote the solution resistance, respectively.

Usually, the equivalent circuit of an electrochemical cell is more complicated than that shown in Fig. 13 and can be found using an electrochemical impedance spectroscopy (EIS) experiment. However, the circuit shown in Fig. 13 is a good starting point for hand calculation and simulation purposes.

In order to maximize the stability of the potential-control loop, A_1 should be a single -stage amplifier that introduces only one low-frequency (dominant) pole into the loop. Thus, we can effectively model A_1 with the following transfer function:

$$A_1(s) = \frac{A_{\rm OL1}}{1+\frac{s}{p_{A1}}} \tag{3}$$

where $A_{\rm OL1}$ is the open-loop gain and p_{A1} is the dominant pole of A_1. Assuming the equivalent circuit of Fig. 13 for the electrochemical cell, we can generate the small-signal model of the potential-control loop, as shown in Fig. 14. g_{m1}, R_{O1}, and C_{O1} represent the transconductance, the output resistance, and the total drain capacitance of M_1, respectively.

If we cut the loop at the noninverting input of A_1 and calculate the open-loop transfer function, we arrive at (4), shown at the bottom of the page, where $\Delta(s)$ is defined as follows:

$$\begin{aligned}\Delta(s) = {} & s^3(R_{S1}R_{\rm WE}C_{\rm WE}R_{\rm CE}C_{\rm CE}R_{O1}C_{O1} \\ & + R_{S2}R_{\rm WE}C_{\rm WE}R_{\rm CE}C_{\rm CE}R_{O1}C_{O1}) \\ & + s^2(R_{S1}R_{O1}C_{O1}R_{\rm CE}C_{\rm CE} \\ & + R_{\rm CE}R_{O1}C_{O1}R_{\rm WE}C_{\rm WE} \\ & + C_{O1}R_{O1}R_{S2}C_{\rm WE}R_{\rm WE} \\ & + C_{O1}R_{O1}C_{\rm WE}R_{S1}R_{\rm WE} \\ & + C_{\rm CE}R_{\rm CE}R_{O1}C_{\rm WE}R_{\rm WE} \\ & + C_{O1}R_{\rm CE}R_{O1}C_{\rm CE}R_{\rm WE} \\ & + R_{S2}R_{\rm CE}C_{\rm CE}R_{O1}C_{O1} \\ & + C_{\rm CE}R_{\rm CE}C_{\rm WE}R_{S1}R_{\rm WE} \\ & + C_{\rm CE}R_{S2}R_{\rm CE}C_{\rm WE}R_{\rm WE}) \\ & + s(R_{S2}R_{\rm CE}C_{\rm CE} + R_{O1}R_{\rm CE}C_{\rm CE} + R_{\rm CE}R_{O1}C_{O1} \\ & + R_{S1}R_{\rm WE}C_{\rm WE} + R_{\rm WE}R_{O1}C_{O1} \\ & + R_{S1}R_{O1}C_{O1} + R_{O1}R_{\rm WE}C_{\rm WE} \\ & + R_{S2}R_{O1}C_{O1} + R_{\rm WE}R_{\rm CE}C_{\rm CE} \\ & + R_{S1}R_{\rm CE}C_{\rm CE} + R_{\rm CE}R_{\rm WE}C_{\rm WE} \\ & + R_{S2}R_{\rm WE}C_{\rm WE}) \\ & + R_{\rm WE} + R_{\rm CE} + R_{S1} + R_{S2} + R_{O1}. \end{aligned} \tag{5}$$

Equation (4) clearly indicates that the loop has two left-half-plane (LHP) zeros located at

$$z_1 = -\frac{1}{C_{\rm WE}(R_{\rm WE}\|R_{S1})} \tag{6}$$

$$z_2 = -\frac{1}{C_{\rm CE}R_{\rm CE}}. \tag{7}$$

However, the denominator of $H(s)$ is too complex to provide a clear insight about the positions of the frequency poles. Therefore, it should be simplified using some realistic assumptions.

The double-layer capacitance existing at an electrode/solution interface is very large (this characteristic is exploited in electrolytic double-layer capacitors, also known as supercapacitors or ultracapacitors [16]). In particular, the double-layer capacitance of WE of our glucose sensor is extremely large due to the use of iridium oxide in its structure [17]. As a result, the first assumption is that C_{O1}, which is the total parasitic capacitance at the drain of M_1, is much smaller than $C_{\rm CE}$ and $C_{\rm WE}$.

The second assumption is that R_{O2}, which is the output resistance of M_1, is very large because the current in M_1 is very small (the current in M_1 is the sensor current that is in the range of a few nanoamperes).

The third assumption is that the solution resistances, i.e., R_{S1} and R_{S2}, are much smaller than $R_{\rm CE}$, $R_{\rm RE}$, and $R_{\rm WE}$.

$$H(s) = \frac{-A_{\rm OL1}(1+sC_{\rm CE}R_{\rm CE})(R_{\rm WE}+R_{S1}+sC_{\rm WE}R_{S1}R_{\rm WE})g_{m1}R_{O1}}{\Delta(s)\left(1+\frac{s}{p_{A1}}\right)} \tag{4}$$

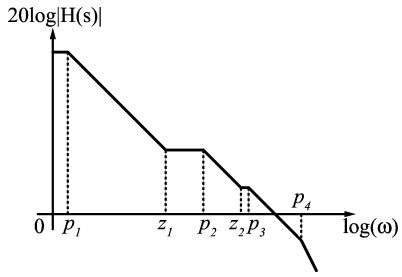

Fig. 15. Relative position of the poles and zeros of the potential-control feedback loop.

Considering the aforementioned assumptions, we can simplify $H(s)$ and approximate the transfer function poles by

$$p_1 \cong -\frac{1}{C_{\rm WE}\left(R_{\rm WE}\|(R_{\rm CE}+R_{O1})\right)} \tag{8}$$

$$p_2 \cong p_{A1} \tag{9}$$

$$p_3 \cong -\frac{1}{C_{\rm CE}(R_{\rm CE}\|R_{O1})} \tag{10}$$

$$p_4 \cong -\frac{1}{C_{O1}(R_{S1}+R_{S2})}. \tag{11}$$

The dominant pole is p_1, which is generated by $C_{\rm WE}$. The next dominant pole is $p_1(=p_{1A_1})$, which is introduced by A_1. Since $R_{CE} \ll R_{O2}$, p_3 is very close to z_2, generating a frequency doublet, for which the frequency of zero is a little less than the pole. p_4 is located at very high frequencies because both C_{O1} and $R_{S1}+R_{S2}$ are small. Fig. 15 graphically shows the relative positions of the poles and zeros of the potential-control loop.

From the previous analysis, we conclude that since $C_{\rm WE}$ and $C_{\rm CE}$ are much larger than the on-chip parasitic capacitances, p_1 is at a much lower frequency compared to the other poles. Therefore, in order to achieve good stability, the nondominant poles must be pushed to higher frequencies. This is particularly important for the first nondominant pole, i.e., p_2, which is the pole of A_1. The analysis also indicates that performing Miller frequency compensation by placing a capacitor between the drain and the gate of M_2, a standard compensation technique, is not appropriate because it pushes p_2 to lower frequencies, bringing it closer to the dominant pole.

In order to push p_2 to higher frequencies, we minimized the parasitic capacitances at the output node of A_1 and also carefully designed the circuit so as not to increase the gain of A_1 more than what is required.

The small-signal equivalent circuit that is produced in an EIS experiment is only valid at the operating cell potential of the electrochemical sensor. During the start-up of a potentiostat, the cell potential moves from the open-circuit potential of the sensor to the desired cell potential. Since the impedance of the sensor is highly dependent on voltage, during the start-up, the impedance may change considerably (a cyclic voltammetry experiment can provide a good insight about the large-signal behavior of an electrochemical sensor). Therefore, the possibility of instability is higher during start-up. As a result, we overstabilized the potentiostat by adding an LHP zero to the potential-control loop using an additional feedforward signal path (as shown in Fig. 16). In Fig. 16, assuming that A_2 and A_3 are unity-gain wideband single-stage amplifiers, we can write the equations of the loop and arrive at the following equation that describes the position of the new LHP zero:

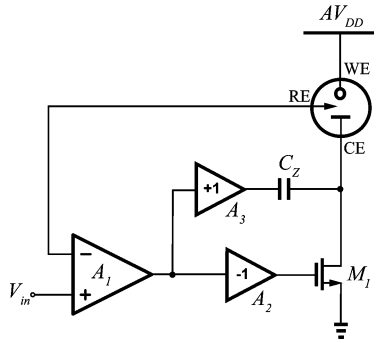

Fig. 16. Addition of an LHP zero to the control loop via a feedforward signal path.

$$z_3 = -\frac{g_{m1}}{C_Z}. \tag{12}$$

Fig. 17 shows the transistor-level schematic of the potentiostat. In order to improve the precision of the current-copying circuit, a cascode structure was used to realize the circuit. Also, the channel length of the transistors in the current-copying circuit was increased.

To minimize the injection of the switching noise from the I-to-F converter to the potentiostat, independent bias circuits were used for the two circuit blocks. Also, independent supply and ground lines were used for the I-to-F converter.

V. Results

As stated in Section IV, because of system design considerations, our potentiostat measures the sensor current by converting it to a pulse signal, for which the time difference between two consecutive pulses, namely, T, is inversely proportional to the sensor current I_F. Thus, in order to characterize the performance of the potentiostat, a circuit emulating a three-electrode electrochemical cell was designed and connected to the potentiostat, and as the output signal, the time difference between the pulses generated at the output of the I-to-F converter was measured using a Tektronix TDS5054B digital oscilloscope.

The circuit used for emulation of the three-electrode electrochemical cell is shown in Fig. 18. The emulated sensor current was varied using a 100-kΩ potentiometer. The current was swept from 1 nA to 1 μA. For the current range of 1–10 nA, the value of $R_{\rm WE}$ was chosen to be 10 MΩ; for the current range of 10–100 nA, the value of $R_{\rm WE}$ was chosen to be 1 MΩ; and for the current range of 100 nA–1 μA, the value of $R_{\rm WE}$ was chosen to be 100 kΩ.

Fig. 19 shows the experimental results demonstrating that the circuit has better than 0.1% accuracy in measuring the sensor current from 1 nA to 1 μA. Fig. 20 shows the output sawtooth waveform of the I-to-F converter for the input current of 600 nA.

The potentiostat was also connected to a microfabricated enzyme-electrode-based glucose biosensor immersed in a nonstirred aerated phosphate buffer solution (pH 7) with 100-mM

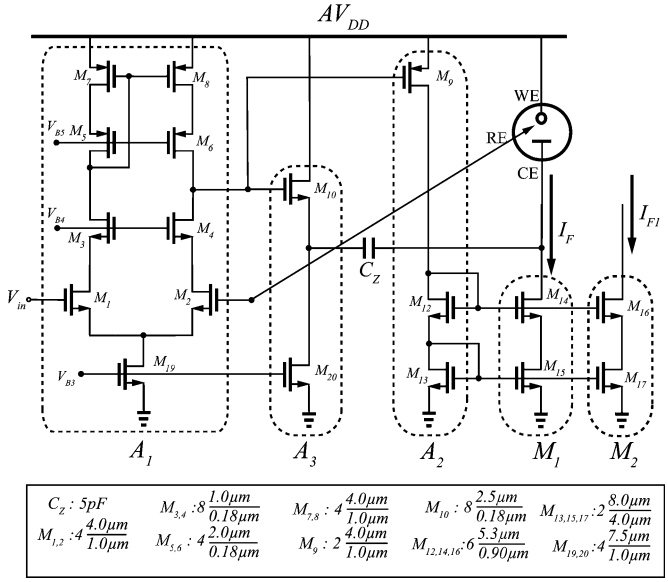

Fig. 17. Transistor-level schematic of the potentiostat.

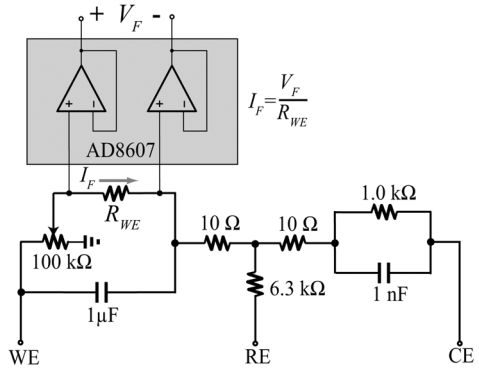

Fig. 18. Schematic of the circuit used for obtaining the calibration curve of the potentiostat.

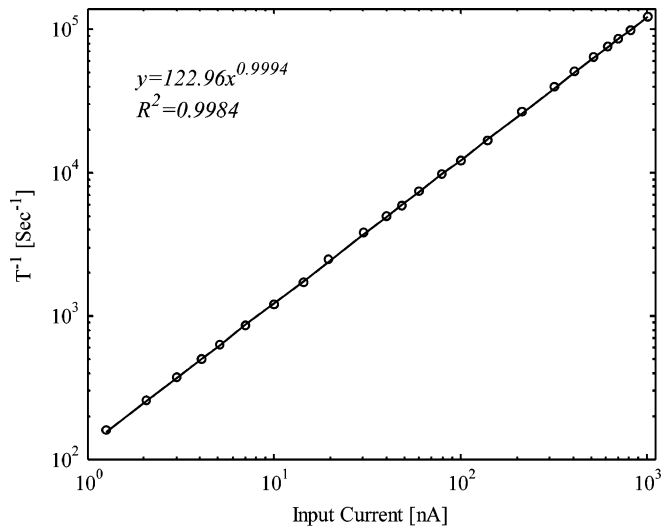

Fig. 19. Measured calibration curve of the potentiostat.

NaCl. The concentration of glucose was increased in steps, and after the sensor current settled to its final value (after about 2 min), the time difference between the pulses at the output of the

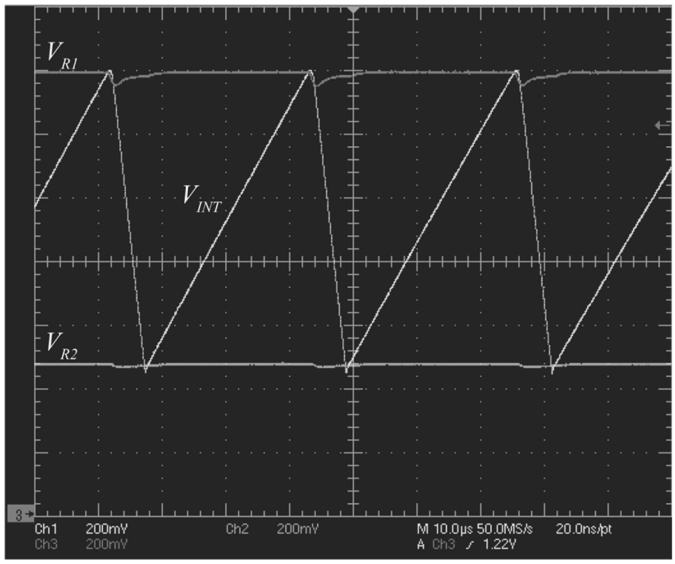

Fig. 20. Output sawtooth waveform of the I-to- F converter for an input current of 600 nA.

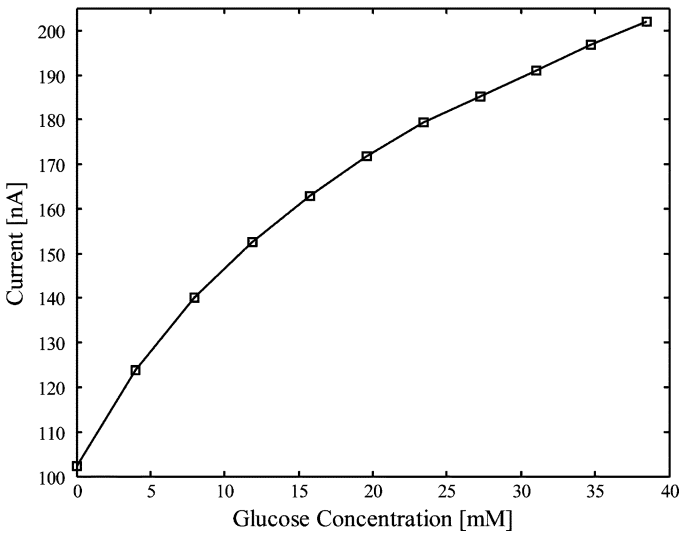

Fig. 21. Measuring glucose concentration using the potentiostat and a three-electrode glucose biosensor.

I-to- F converter was measured at each step. Fig. 21 shows the current measured by the potentiostat against different glucose concentrations. The saturating response of the glucose biosensor is due to the fact that we had not placed a diffusion-limiting layer over the glucose biosensor; thus, the sensor was functioning in a mass-transport-limited regime.

The aforementioned performance of the potentiostat was achieved with a very low power consumption and a very small die area. The total power consumption of the potentiostat and I-to- F converter is about 50 μW (from a 1.8-V supply voltage). Fig. 22 shows a micrograph of the fabricated potentiostat circuit. The total occupied active area by the potentiostat and I-to- F converter is about 0.02 mm^2.

VI. Conclusion

In this paper, we have presented a new class of potentiostat circuits in which a current-copying circuit, similar to a current

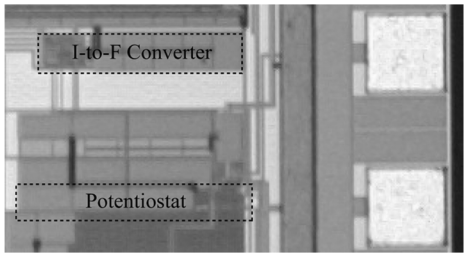

Fig. 22. Microphotograph of the potentiostat.

mirror, was used to generate a mirror image of the sensor current and then process and measure the copied current. These new circuits have a number of important advantages over the previously published topologies. First, the WE in the new potentiostats is connected to a true ground, making it less prone to noise and interference pickup. Second, the circuit has very low noise because it uses fewer active and passive components for measuring current. Third, the circuit consumes very low power, making it a suitable choice for portable applications. Fourth, very small currents can be measured by simply switching the current measurement resistor to higher values, and this switching to a higher resistor does not have any effect on the stability of the potential-control loop. Finally, the new potentiostat circuits do not have headroom voltage issues, which plague some of the existing circuits.

To demonstrate the feasibility of our proposed circuit, an electronic potentiostat based on the new topology was implemented using the TSMC 0.18-μm CMOS process, and the measurement results were presented, demonstrating excellent linearity with very low power consumption and very small die area.

In addition, we have presented a very thorough analysis of the stability of the potential-control feedback loop.

ACKNOWLEDGMENT

The authors would like to thank Prof. V. I. Birss and A. S. Jhas for their collaboration in testing the integrated potentiostat, CMC Microsystems for providing the tools and fabrication technology for our use, and the reviewers for their comments and suggestions.

REFERENCES

[1] J. Bard and L. R. Faulkner, *Electrochemical Methods: Fundamentals and Applications*, 2nd ed. New York: Wiley, 2001.

[2] M. M. Ahmadi and G. A. Jullien, , K. Iniewski, Ed., "Circuits for amperometric electrochemical sensors," in *VLSI Circuit Design for Biomedical Applications*. Norwood, MA: Artech House, 2008.

[3] L. Busoni, M. Carla, and L. Lanzi, "A comparison between potentiostatic circuits with grounded work or auxiliary electrode," *Rev. Sci. Instrum.*, vol. 73, no. 4, pp. 1921–1923, Apr. 2002.

[4] R. Doelling, "Potentiostats," in *Bank Elektronik Application Note*, 2nd ed. Clausthal-Zellerfeld, Germany: Bank Elektroni–Intelligent Controls GmbH, Mar. 2000.

[5] R. Greef, "Instruments for use in electrode process research," *J. Phys. E, Sci. Instrum.*, vol. 11, no. 1, pp. 1–12, Jan. 1978.

[6] E. Wilkins and P. Atanosov, "Glucose monitoring: State of the art and future possibilities," *Med. Eng. Phys.*, vol. 18, no. 4, pp. 273–288, Jun. 1996.

[7] R. Kakerow, H. Kappert, E. Spiegel, and Y. Manoli, "Low-power single-chip CMOS potentiostat," in *Proc. 8th Int. Conf. Solid-State Sens., Actuators*, 1995, pp. 142–145.

[8] R. Reay, S. Kounaves, and G. Kovacs, "An integrated CMOS potentiostat for miniaturized electroanalytical instrumentation," in *Proc. IEEE ISSCC*, 1994, pp. 162–163.

[9] A. Gore, S. Chakrabartty, S. Pal, and E. C. Alocilja, "A multichannel femtoampere-sensitivity potentiostat array for biosensing applications," *IEEE Trans. Circuits Syst. I, Reg. Papers*, vol. 53, no. 11, pp. 2357–2363, Nov. 2006.

[10] M. Stanacevic, K. Murari, A. Rege, G. Cauwenberghs, and N. V. Thakor, "VLSI potentiostat array with oversampling gain modulation for wide-range neurotransmitter sensing," *IEEE Trans. Biomed. Circuits Syst.*, vol. 1, no. 1, pp. 63–72, Mar. 2007.

[11] H. S. Narula and J. G. Harris, "A time-based VLSI potentiostat for ion current measurements," *IEEE Sensors J.*, vol. 6, no. 2, pp. 239–247, Apr. 2006.

[12] R. Genov, M. Stanacevic, M. Naware, G. Cauwenberghs, and N. Thakor, "16-channel integrated potentiostat for distributed neurochemical sensing," *IEEE Trans. Circuits Syst. I, Reg. Papers*, vol. 53, no. 11, pp. 2371–2376, Nov. 2006.

[13] S. Ayers, K. D. Gillis, M. Lindau, and B. A. Minch, "Design of a CMOS potentiostat circuit for electrochemical detector arrays," *IEEE Trans. Circuits Syst. I, Reg. Papers*, vol. 54, no. 4, pp. 736–744, Apr. 2007.

[14] S. M. R. Hasan, "Stability analysis and novel compensation of a CMOS current-feedback potentiostat circuit for electrochemical sensors," *IEEE Sensors J.*, vol. 7, no. 5, pp. 814–824, May 2007.

[15] M. M. Ahmadi and G. Jullien, "A low power CMOS potentiostat for bioimplantable applications," in *Proc. 5th IWSOC*, 2005, pp. 184–189.

[16] *"Get the Lowdown on Ultracapacitors,"* Electronic Design, Nov. 15, 2007, Tuite, ED Online ID #17465.

[17] V. I. Birss, Private Communications, University of Calgary, Dec. 2005.

Mohammad Mahdi Ahmadi (S'05–M'07) received the B.Sc. degree in biomedical engineering (with highest honors) from Shahid Beheshti University, Tehran, Iran, in 2000, the M.Sc. degree in electronic engineering from Sharif University of Technology, Tehran, in 2002, and the Ph.D. degree in electrical engineering from the University of Calgary, Calgary, AB, Canada, in 2007. His Ph.D. research was on developing a wireless implantable microsystem for continuous blood glucose monitoring.

Since November 2007, he has been a Member of the R&D Group with Sound Design Technologies Ltd., Burlington, ON, Canada. His research interests include analog, mixed-signal, and RF IC design for biomedical and communication applications. He has also conducted research in the areas of BioMEMS and biomedical microsystems.

Dr. Ahmadi has received awards in the 44th ISSCC/DAC and the Third Analog Devices Student Circuit Design Contests. He was also the winner of the Clearest Message Award at the 2006 Alberta Biomedical Engineering Conference and the recipient of the Robert B. Paugh Memorial Scholarship in Engineering in 2006.

Graham Jullien (M'71–SM'83–F'03–LF'08) received the B.Tech. degree from Loughborough University, Leicestershire, U.K., in 1965, the M.Sc. degree from Birmingham University, Birmingham, U.K., in 1967, and the Ph.D. degree from the University of Aston, Birmingham, U.K., in 1969.

He recently retired as iCORE Chair of Advanced Technology Information Processing Systems (ATIPS) and Director of the ATIPS Laboratories, University of Calgary, Calgary, AB, Canada. He retains the position of Professor Emeritus in the Department of Electrical and Computer Engineering. His long-term research interests include integrated circuits (including systems-on--chip), VLSI signal processing, computer arithmetic, high-performance parallel architectures, and number-theoretic techniques. Since taking up his chair position at Calgary, he expanded his research interests to include security systems, nanoelectronic technologies, and biomedical systems. He was also instrumental, along with his colleagues, in developing an Integration Laboratory cluster to explore next-generation integrated microsystems. He has published more than 390 papers in refereed technical journals and conference proceedings and has served on the organizing and program committees of many international conferences and workshops over the past 35 years.

Dr. Jullien is a Life Fellow of the Engineering Institute of Canada and, until recently, was a member of the Boards of Directors of DALSA Corporation, CMC Microsystems, and Micronet R&D. He was the General Chair for the IEEE International Symposium on Computer Arithmetic in Montpellier in 2007 and was a Guest Coeditor for the IEEE Proceedings Special Issue on System-on-Chip: Integration and Packaging, June 2006.